RESEARCH ARTICLE

Synthesis, Functionalized and Characterization of Magnetic Fe_3O_4 Nanoparticles Protected with MCM-41 Mesoporous

Ardeshir Shokrollahi*, Salimeh Abbasi, Shaghayegh Mohammadpour Shirazi

Department of Chemistry, Yasouj University 75918-74831, Yasouj, Iran

Corresponding author: E-mail: ashokrollahi@yu.ac.ir

DOI: 10.5185/amlett.2020.081550

In this article the synthesis of Fe_3O_4@MCM-41@NH-2,6-pydc as good adsorbent with potential of many applications, by coprecipitation method, was reported. For this purpose, Fe_3O_4 was synthesized, then protected with MCM-41 as a shell. Afterward, Fe_3O_4@MCM-41 functionalized by 2,6-pyridine dicarboxylic acid (pydc) after modifying by 3-aminopropyl trimethoxysilane (APTMS). This adsorbent characterized by means of X-ray diffraction (XRD), Fourier transform infrared spectroscopy (FT-IR), energy dispersive X-ray (EDX), scanning electron microscope (SEM), Brunauer–Emmett–Teller (BET), differential thermal analysis (DTA), thermogravimetric analyses (TGA) and derivative thermogravimetric (DTG). The vibrating sample magnetometer (VSM) has been used to investigate its magnetic properties.

Introduction

Magnetic nanoparticles and their functionalized, attract plenty attention through their markable usages in different field such as biotechnology [**1**], metal ion extraction [**2**], carriers for targeted drug delivery [**3**], optical imaging [**4**], electronic [**5**], magneto resistance [**6**] and catalyst [**7**]. In which magnetic nanoparticles are present, specially for Fe_3O_4 nanoparticles have individual, features including superparamagnetism, high surface area, large surface-to-volume ratio, facile separation by external magnetic fields [**3, 8-10**]. Also due to their good biocompatibility and low toxicity, Fe_3O_4 nanoparticles are the most preferable [**11-14**]. However, Fe_3O_4 nanoparticles are inclined to aggregate, oxidize and decompose, and thus it is essential to protect their surfaces [**15**]. The purpose of shell coating of nude magnetic nanoparticles in core–shell structure is insulatoring the magnetic core versus the environment [**16**].

One important clansman of the M41S mesoporous molecular sieve family is mesoporous MCM-41, with a hexagonal arrangement of uniform channels of 15–100 A° diameter. The MCM-41 synthesis process begins by utilizes quaternary alkylammonium salts like cetyltrimethylammonium bromide (CTAB) in an aqueous solution under basic conditions. The ionic surfactant form spherical micelles that form template by forming a liquid crystalline phase [**17**]. The hydrolysis and condensation of silica precursors, as an example tetraethylorthosilicate (TEOS) forms a solid silicate mesostructure around the template because of electrostatic interactions between the negatively charged silica species and head groups of the surfactant, or by hydrogen bonding interactions. ultimately the template is removed by calcination after formation of the silicate mesostructure [**18**].

Due to its very high surface area (up to 1000 m^2/g), its narrow size pore distribution and thermal stability (up to 800°C) [**19,20**], it will be an assorted support material for Fe_3O_4 nanoparticles.

The surface modification of magnetic nanoparticles could improve selectivity, dispersity and biocompatibility, that could appreciably simplify its beneficiary [**21**]. Because of hydrophilic surfaces of silica-coated magnetic nanoparticles, this shell alone cannot stabilize the nanoparticles in a specific qualification but it could be easily modified with other funcional groups [**22**].

This material has been prepared by precipitation [**23**], co-precipitation [**24**] and hydrothermal [**25**] methods. Amid these methods, chemical co-precipitation may be the most encouraging, due to its facility and efficiency [**16**].

Using differing polymers with different functional groups for functionalizing magnetic Fe_3O_4 nanoparticles and MCM-41 mesoporous can augmented its adsorption capacity and selectivity [**26**]. So the cited nanoparticles and mesoporous was used for many purposes such as solid phase extraction [**27**], removal of ions [**28**], delivery of biomolecules [**29**] and etc.

By functionalizing of magnetic Fe_3O_4 nanoparticles or MCM-41 mesoporous, they could be used to adsorb, preconcentrate and extract the cationic species analogous protonated form of drug and amines, basic and cationic dyes, amino acids and metal ions. So because of the good properties of carboxylate positions for interactions with organic and inorganic cations, it is suitable for functionalizing. Bygone research by Shokrollahi and colleagues represent pleasant interactions between 2,6-pyridine dicarboxylic acid (pydc) and different bases like piperazines [**30**] amino pyridines [**31**] and acridines [**32**]. Based on the previous researches, it is anticipated that

nanoparticles functionalized by pydc could be utilized as a proper surface for the adsorption, extraction and preconcentration of organic and inorganic compounds. According our previous study [**33**], Fe_3O_4@SiO_2-NH-2,6 pydc was synthesized as a good adsorbent in easy separation, but the adsorption capacity of it can be improved by coating with MCM-41.

The purpose of this study is, using co-precipitation method for synthesis Fe_3O_4 and afterward form an outer shell by coating MCM-41. Then the surface of these nanoparticles is loading through the grafting by APTMS and ultimately functionalized by pydc.

Experimental

Materials

Ferrous chloride tetrahydrate ($FeCl_2{\cdot}4H_2O$), ferric chloride hexahydrate ($FeCl_3{\cdot}6H_2O$), cetyltrimethyl ammonium bromide (CTAB), ammonium hydroxide (25%, w/w), tetraethyl orthosilicate (TEOS), (3-aminopropyl) trimethoxysilane (APTMS), Toluene (C_7H_8), 2,6-pyridine dicarboxylic acid (2,6-pydc), ethanol (C_2H_5OH, 99.7%), dichloromethane (CH_2Cl_2) and triethylamine ($N(CH_2CH_3)_3$), methyl green, mallachite green, and phenylalanine were purchased from Merck chemical company (Darmstaadt, Germany). Thionyl chloride ($SOCl_2$) was purchased from Sigma-Aldrich Company (St. Lous, Germany).

Apparatus

XRD spectra were taken on a Philips XPERT MPD X-ray diffractometer with Cu-Kα radiation (λ = 1.5406 Å) and scanning mode from 0° (2θ) to 80° (2θ). IR spectra were obtained in the range 400 to 4000 cm^{-1} using KBr pellets on a Jasco 460 FT-IR spectrometer. The magnetic properties of Fe_3O_4 and Fe_3O_4@MCM-41-NH_2-2,6pydcwere measured with VSM (MDKB, Daghigh Meghnati kavir Co., Iran). Scanning Electron Microscope model Sigma VP from ZEISS Company was applied for the morphological structure of nanoparticle. The specific surface, the pore size distribution, and the total pore volume were determined from N2 adsorption–desorption isotherms obtained by using a Micrometrics ASAP 2020. The TGA and DTA were done on a Perkin Elmer Pyres diamond TG/DTA instrument in N_2 atmosphere at a heating rate of 20°C min^{-1} from 28 to 887°C. An ultrasonic bath with heating system (Tecno-GAZ SPA Ultrasonic System, Italy) at 40 kHz of frequency and 130 W of power.

Synthesis of Fe_3O_4

Co-precipitation technique has been used to prepare magnetic Fe_3O_4 nanoparticles. $FeCl_2{\cdot}4H_2O$ (4.0g) and $FeCl_3{\cdot}6H_2O$ (10.8g) were dissolved in 100 mL double distilled water under nitrogen purging. Ammonia (50.0 mL, 25%) was added into the solution dropwise to adjust the pH value to approximately 9.0 and the brown color solution turned out to black. After vigorously stirred for 30 min, the temperature should be 70°C. The precipitate was collect by powerful external magnet and was washed with double distilled water and ethanol for several times. The resulting black powder was dried in an oven at 40°C.

Synthesis of Fe_3O_4@MCM-41

For the preparation of Fe_3O_4 at the mobile composition of matter No. 41 (MCM-41), 0.3g of Fe_3O_4 was dispersed in absolute ethanol (210mL) under sonication for 30 min and CTAB (1.5g) was stirred in 180mL of deionized water for 30 min at room temperature. Two above solutions were mixed followed by an addition dropwise of tetraethylorthosilicate (TEOS; 3mL), ammonia (15 mL, 25%) and stirred at room temperature for 24 h. The obtained Fe_3O_4 nanoparticles coated with mesoporous silica were washed with ethanol (total 40mL) and acetone (total 30mL) several times, separated magnetically and dried at 50°C. The dried sample was finally calcinated at 500°C for 9h for the extraction of template CTAB.

Synthesis of Fe_3O_4@MCM-41-NH_2

For surface modification of the Fe_3O_4@MCM-41 with APTMS, APTMS (1.0mL) and Fe_3O_4@MCM-41 (about 1.0g) were added in toluene (20mL). The mixture was permitted to react by refluxing at 110 °C for 24 h. After this time, the production Fe_3O_4@MCM-41-NH_2 were separated magnetically, and washed with toluene (20mL) and ethanol (20mL). The Fe_3O_4@MCM-41-NH_2 was dried in an oven at 50°C.

Synthesis of Fe_3O_4@MCM-41-NH -2,6-pydc

The solution of 2,6-pyridine dicarboxylic acid (0.5g) in $SOCl_2$ (8.72 mL) was heated to reflux (70°C) and kept at reflux for 18 h. After the remaining $SOCl_2$, was evaporated of system, Fe_3O_4@MCM-41-NH_2 (0.8g), triethylamine (43.63µL) and CH_2Cl_2 (8.72mL) were added to a beaker respectively, then the reaction mixture was stirred at room temperature for 6 h. The product (Fe_3O_4@MCM-41-NH -2,6-pydc) was filtered and washed with ethanol then was dried in an oven at 50°C.

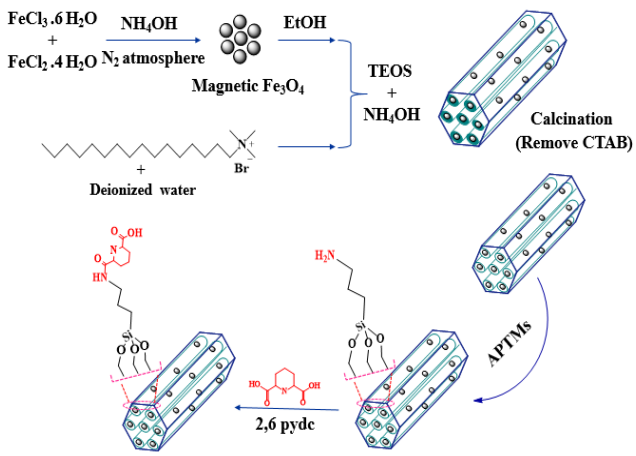

Fig. 1. Schematic representative for the preparation of Fe3O4@MCM-41-NH-2,6-pydc nanoparticles.

Characterizations

X-ray diffraction (XRD), fourier transform infrared spectroscopy (FT-IR), scanning electron microscope (SEM), **e**nergy dispersive X-ray (EDX), vibrating sample magnetometer (VSM), Brunauer–Emmett–Teller (BET), thermogravimetric analysis (TGA), derivative thermogravimetric (DTG) and differential thermal analysis (DTA) were used to check out and distinction of synthesized magnetic nanoparticles.

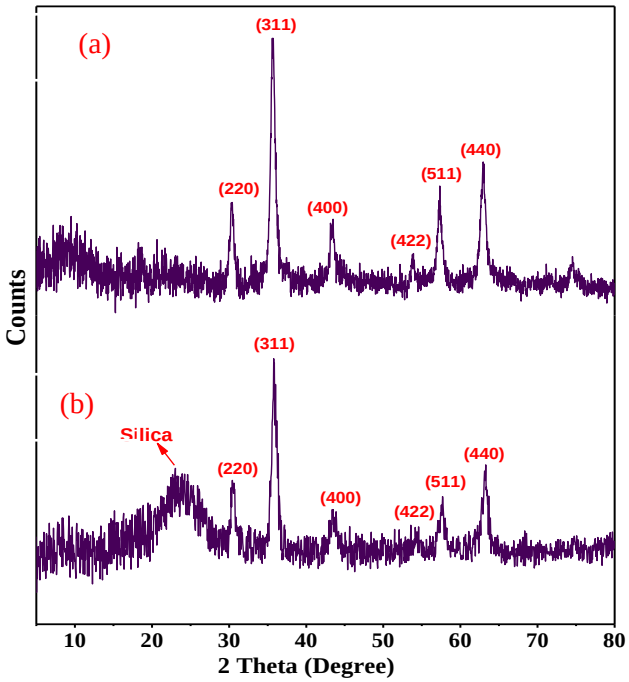

Fig. 2. XRD patterns of bare Fe_3O_4 (a) Fe_3O_4@ MCM-41-NH-2,6-pydc (b) nanoparticles.

Results and discussion

XRD analysis

To recognition the crystalline structure of the synthesized nanoparticles, it was analyzed by X-ray diffraction from 0° (2θ) to 80° (2θ) (**Fig. 2**). **Fig. 2a**, shows six characteristic peaks indicated a crystallized structure at 2θ of 30.52°, 35.81°, 43.50°, 53.87°, 57.61° and 63.18° which was dedicated to the Fe_3O_4 crystal plan (200), (311), (400), (422), (511) and (440), respectively. These results were compared to the reference No 96-900-5842, confirming the highly spinal structure. **Fig. 2b** shows the XRD spectrum of Fe_3O_4@MCM-41-NH-2,6pydc and it's similar to **Fig. 2a** except a broad diffusion peak at 2θ of 19.54° related to the SiO_2 amorphous phase (Ref. No 96-210-1989). These results revealed that the initial crystallographic structure of Fe_3O_4, was preserved perfectly during the surface modification process.

FT-IR analysis

As seen in **Fig. 3** the functional groups in the synthesized nanoparticles were recognized by FT-IR analysis. The presence of vibration band at 586 cm^{-1} demonstrates the existence of Fe_3O_4 and it is observed in all three spectra. The vibration band that observed at 1064 cm^{-1} (**Fig. 3b** and **Fig. 3c**) refers to SiO_2 and shows that Fe_3O_4 protected with MCM-41. Also, the acidic OH peak appearance at 3409 cm^{-1}. The N-H stretching vibration band related to N-H group of 3-aminopropyl can be intended at 3300-3400 cm^{-1}. But it is noteworthy the apparition of a broad peak instead of a sharp peak, is regarding to the attendance of unlimited OH groups on the surface. The presence of pyridine ring can be confirmed by the peak at 1454-1564 cm^{-1} that refers to C=C and C=N (**Fig. 3c**). The absorption band that assigned to C=O is demonstrated at 1621 cm^{-1}. Finally, we conclude that Fe_3O_4@MCM-41-2,6 pydc was successfully synthesized.

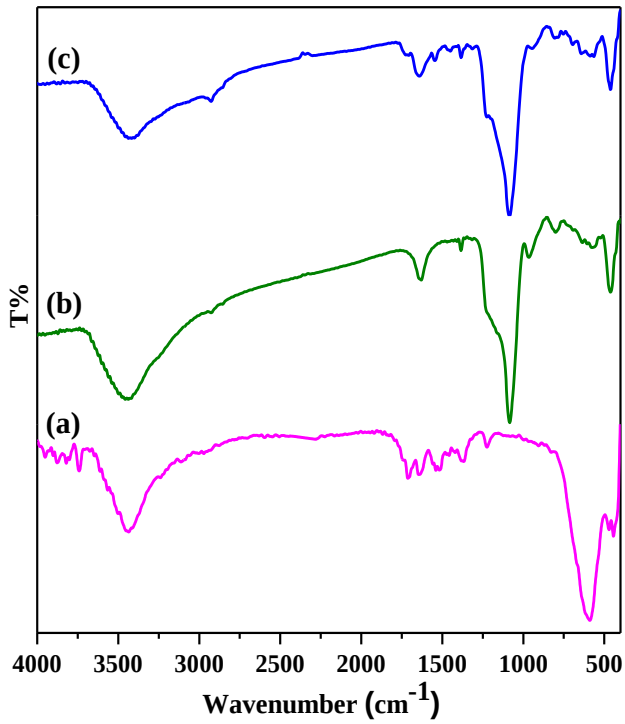

Fig. 3. FT-IR spectra of Fe_3O_4 (a) Fe_3O_4@ MCM-41(b) Fe_3O_4@MCM-41-NH-2,6-pydc (c) nanoparticles.

SEM analysis

The scanning electron microscopy (SEM) images of the Fe_3O_4@MCM-41-NH -2,6-pydc (**Fig. 4**) in two magnification showed micro size of smooth spherical particles.

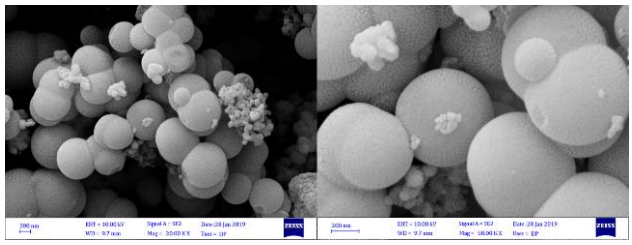

Fig. 4. SEM images of the Fe_3O_4@MCM-41-NH-2,6-pydc nanoparticles.

EDX analysis

The EDX spectrum of Fe_3O_4@MCM-41-NH-2,6pydc (**Fig. 5**), showed an elemental composition of Fe, Si, O, C and N for the material.

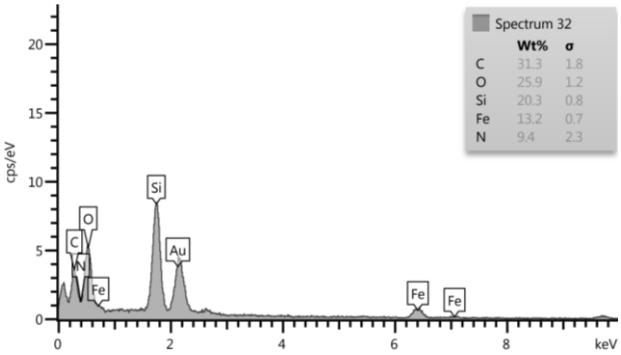

Fig. 5. EDX spectra of Fe_3O_4@ MCM-41-NH-2,6-pydc nanoparticles.

VSM analysis

The magnetic parameters of the Fe_3O_4 and Fe_3O_4@MCM-41-NH -2,6-pydc were measured out at room temperature by vibrating sample magnetometer (VSM) analysis (Error! Reference source not found.). Saturated magnetic property (Ms), amount of residual or magnetic stability (Mr) and negative or reversing force (Hc), are magnetic parameters that have been obtained from the curves and shown in **Table 1**. As seen in the curves of MS for different materials were weakened, indicating that Fe_3O_4 nanoparticles were coated by the non-magnetic material. So the decrease in magnetic property shows successful modification of Fe_3O_4 nanoparticles with MCM-41 mesoporous and the Ms for Fe_3O_4 ranges from 57.47 to 7.80 emu/g diminished. Consequently, the plot shows that the Fe_3O_4@MCM-41-NH -2,6-pydc exhibit a typical super paramagnetic behavior due to their small magnetic stability.

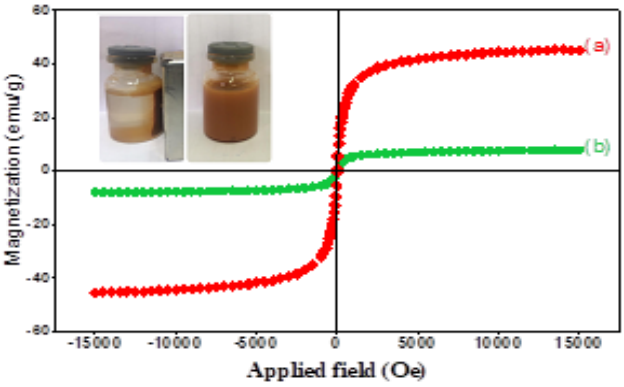

Fig. 6. VSM curves of Fe_3O_4 (a), Fe_3O_4@MCM-41-NH -2,6-pydc (b) nanoparticles.

Table 1. Magnetic parameters of Fe_3O_4 and Fe_3O_4@MCM-41-NH -2,6-pydc nanoparticles.

Magnetic parameters	Fe_3O_4	Fe_3O_4@MCM-41-NH -2,6-pydc
M_s (emu/g)	57.474	7.8
M_r (emu/g)	1.617	0.14
H_c (Oe)	14.634	5.7

BET analysis

Nitrogen adsorption/desorption isotherm and the corresponding pore size distribution of Fe_3O_4@MCM-41-NH-2,6pydc are shown in **Fig. 7** Fig. **8**. Isotherm curves in **Fig. 7** can be attributed to type IV according to the IUPAC classification, and the curves confirmed that after the modification, the samples maintained their mesoporous structures [**34**]. The corresponding pore size distribution of the sample (**Fig. 8**) showed that the pore size was between 1–100 nm. The surface area, pore volume and pore size are shown in **Table 2**. These result in comparing the reports about Fe_3O_4@MCM-41, has confirmed that the functionalizing with 2,6-pydc decreased the BET surface area, pore volume and pore size. However the purposed adsorbent has better properties than the similar cases in reports [**35**].

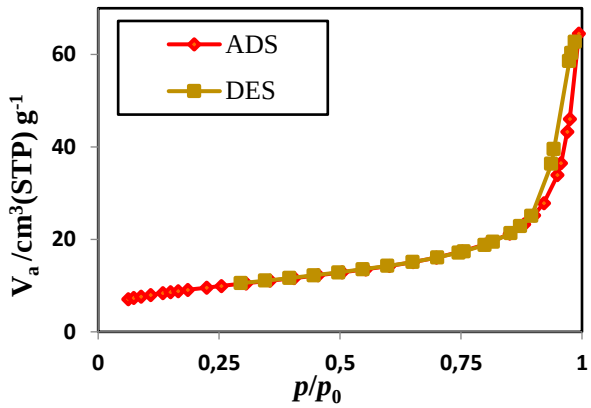

Fig. 7. Nitrogen adsorption/desorption isotherms of Fe_3O_4@MCM-41-NH-2,6-pydc.

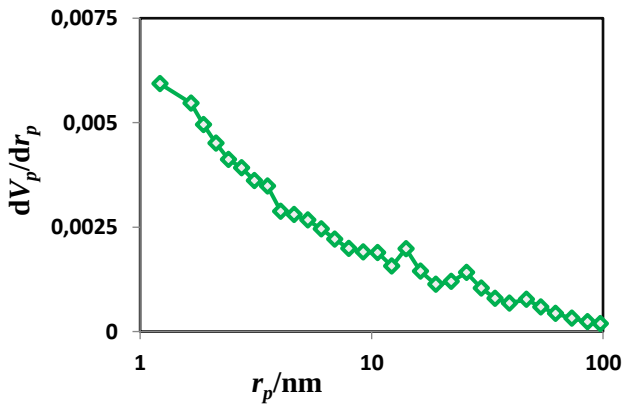

Fig. 8. Pore size distribution of Fe_3O_4@MCM-41-NH-2,6-pydc.

Table 2. Surface area, pore volume and pore size of Fe_3O_4@SiO2-NH -2,6-pydc.

Sample	Fe_3O_4@MCM-41-NH -2,6-pydc
Surface area/(m^2g^{-1})	23.39
Pore volume/(cm^3g^{-1})	0.09
Pore size/nm	1.22

Thermal stability analysis

TGA, DTG and DTA was used for appraising the thermal stability of synthesized Fe_3O_4@MCM-41-NH -2,6-pydc. The TGA curves (W vs. T and W% vs. T scales) of Fe_3O_4 nanoparticles and Fe_3O_4@MCM-41-NH-pydc are shown in **Fig. 9** and **Fig. Fig. *10*** respectively. According to the graphs, there are three decomposition peaks that the first one in the range 28-147°C alluded to evaporation of solvent that adsorbed on the surface of nanoparticles. Two other weight loss in the range of 147-302 and 302-678°C can be alluded to decomposition of pydc and APTMS. Also these changes are shown distinctly in the DTG. DTA [**36**], approved these reasoning. So there are peaks in DTA in places that lose weight in DTG were happened. Albeit heat events that are regarding to change in energy can be detectable with DTA, the other heat events that are related to change in mass cannot be detectable.

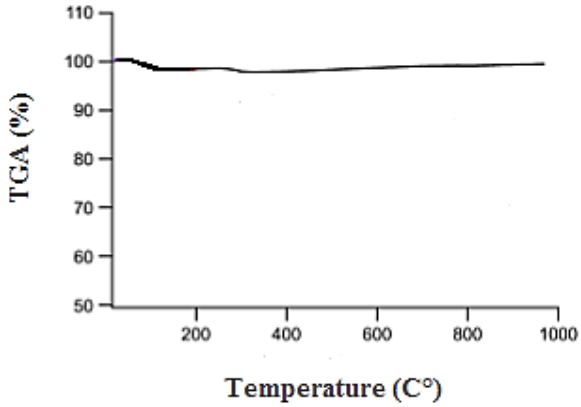

Fig. 9. TG thermograms of Fe_3O_4

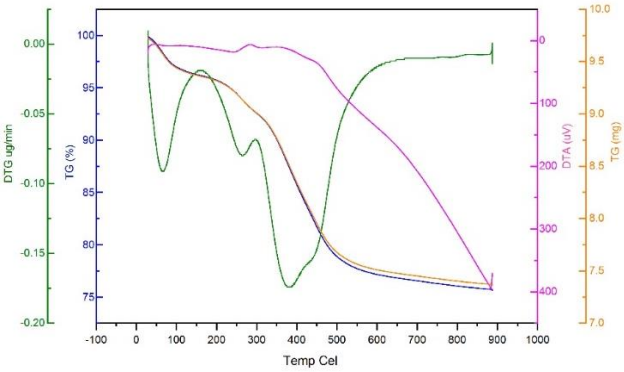

Fig. 10. TG thermograms, DTG and DTA of Fe_3O_4@MCM-41-NH -2,6-pydc nanoparticles.

Ability of Fe_3O_4@MCM-41-NH -2,6-pydc as an adsorbent

The ability of the cited mesoporous was tested by using as an adsorbent for removal or preconcentration of some dyes and amino acids such as methyl green, malachite green and phenylalanine. It seems that this mesoporous has good absorption capacity and it is a good adsorbent for removing of methyl green and malachite green. Also it is an efficient adsorbent for preconcentration and extraction of these dyes and phenylalanine amino acid in low level concentrations.

Conclusions

Achievements of this research, is synthesis of magnetic Fe_3O_4 nanoparticle and increasing of its stability with MCM-41 mesoporous. Also using APTMS as a modifier can improve dispersity and biocompatibility. The functionalizing of purpose nanoparticles with 2,6-pydc can raise the selectivity. Resulting is, formation Fe_3O_4@MCM-41-2,6-pydc as a benefit and optional adsorbent for purposes such as removal, separation and extraction of organic and inorganic species. XRD, FT-IR, EDX and thermal analyses confirm this synthesis and VSM curves shows, though the modifier decreased magnetism, still it has magnetic properties. Fe_3O_4@MCM-41-2,6-pydc is a good adsorbent due to easy separation and high capacity. Also the potency to interact with cationic species can be facilitated by functionalizing with carboxylate groups.

Although the new synthesized adsorbent have less magnetic feature toward Fe_3O_4@SiO_2-NH-pydc [**33**] but because of existence MCM-41 in structure it has more surface area. So it is an adsorbent that competitive with Fe_3O_4@SiO_2-NH-pydc and functionalized MCM-41 and in addition appropriate surface area, it is easily separated from analyte. If we take look at some similar synthesis of other researchers we will come to this conclusion that our syntheses have desirable properties **[35,37**] and functionalized by 2,6-pydc prepares it for our intended purposes.

The adsorption capacity of the Fe_3O_4@MCM-41-2,6pydc examined by removing or preconcentration of some dyes and amino acids including methyl green, malachite green and phenylalanine. The results show the excellent adsorption capacity compare to similar nanoparticles [**38**].

Gratitude

Acknowledgement to the supports of this research by Yasouj University.

Keywords

Fe_3O_4@MCM-41@NH-2,6-pydc, APTMS, Modification.

Received: 12 January 2020
Revised: 20 April 2020
Accepted: 27 April 2020

References

1. Zhou, X.; Shi, Y.; Ren, L.; Bao, S.; Han, Y.; Wu, S.; et al., *J. Solid State Chem.*, **2012**, *196*, 138.
2. Wang, J.; Zheng, S.; Shao, Y.; Liu, J.; Xu, Z.; Zhu, D.; *J. Colloid Interface Sci.*, **2010**, *349*, 293.
3. Sun, C.; Lee, J.S.; Zhang, M.; *Adv. Drug Delivery Rev.*, **2008**, *60*, 1252.
4. Lu, P.; Zhang, J. L.; Liu, Y. L.; Sun, D. H.; Liu, G. X.; Hong, G. Y.; et al., *Talanta*, **2010**, *82*, 450.
5. Gilbert, B.; Katz, J.E.; Denlinger, J.D.; Yin, Y.; Falcone, R.; Waychunas, G.A.; *The Journal of Physical Chemistry C*, **2010**, *114*, 21994.
6. Shoshi A.; Schotter, J.; Schroeder, P.; Milnera, M.; Ertl, P.; Heer, R.; et al., *Biosensors and Bioelectronics*, **2013**, *40*, 82.
7. Rostamnia S.; Doustkhah, E.; *J. Magn. Magn. Mater.*, **2015**, *386*, 111.
8. Laurent S.; Forge, D.; Port, M.; Roch, A.; Robic, C.; Vander Elst, L.; et al., *Chem. Rev.*, **2008**, *108*, 2064.

9. Gao H.; Zhao, S.; Cheng, X.; Wang, X.; Zheng, L.; *Chem. Eng. J.*, **2013**, *223*, 84.
10. Xu P.; Zeng, G.M.; Huang, D.L.; Lai, C.; Zhao, M.H.; Wei, Z.; et al., *Chem. Eng. J.l*, **2012**, *203*, 423.
11. Jain T.K.; Reddy, M.K.; Morales, M.A.; Leslie-Pelecky, D.L.; Labhasetwar, V.; *Mol. Phar.*, **2008**, *5*, 316.
12. Liu Y.; Jia, S.; Wu, Q.; Ran, J.; Zhang, W.; Wu, S.; *Catal. Comm.*, **2011**, *12*, 717.
13. Gao J.; Gu, H.; Xu, B.; *Acc. Chem. Res.*, **2009**, *42*, 1097.
14. Shubayev V.I.; Pisanic II, T.R.; Jin, S.; *Adv. Drug Delivery Rev.*, **2009**, *61*, 467.
15. Zhou Z.; Piepenbreier, F.; Marthala, V.R.; Karbacher, K.; Hartmann, M.; *Catal. Today*, **2015**, *243*, 173.
16. Lu A.H.; Salabas, E.e.L.; Schüth, F.; *Angew. Chem. Int. Ed.*, **2007**, *46*, 1222.
17. Sayari A.; *Chem. Mater.*, **1996**, *8*, 1840.
18. Alahmad S.; *Orient. J. Chem.*, **2012**, *28*, 01.
19. Pérez C.N.; Moreno, E.; Henriques, C.; Valange, S.; Gabelica, Z.; Monteiro, J.; *Microporous Mesoporous Mater.*, **2000**, *41*, 137.
20. Beck J.S.; Vartuli, J.; Roth, W.J.; Leonowicz, M.; Kresge, C.; Schmitt, K.; et al., *J. Am. Chem. Soc.*, **1992**, *114*, 10834.
21. Prozorov T.; Kataby, G.; Prozorov, R.; Gedanken, A.; *Thin Solid Films*, **1999**, *340*, 189.
22. Ulman A.; *Chem. Rev.*, **1996**, *96*, 1533.
23. Yao, Y.; Miao, S.; Yu, S.; Ma, L.P.; Sun, H.; Wang, S.; *J. Colloid Interface Sci.*, **2012**, *379*, 20.
24. Utkan, G.G.; Sayar, F.; Batat, P.; Ide, S.; Kriechbaum, M.; Pişkin, E.; *J. Colloid Interface Sci.*, **2011**, *353*, 372.
25. Mizutani, N.; Iwasaki, T.; Watano, S.; Yanagida, T.; Tanaka, H.; Kawai, T.; *Bull. Mater. Sci.*, **2008**, *31*, 713.
26. Jiao, Y.; Jiang, J.; Zhang, H.; Shi, K.; Zhang, H.; *Eur. Polym. J.*, **2014**, *54*, 95.
27. Molaei, R.; Tajik, H.; Moradi, M.; *Food Control*, **2019**, *101*, 1.
28. Alizadeh, K.; Khaledyan, E.; Mansourpanah, Y.; *J. Water Environmental Nanotech.*, **2018**, *3*, 243.
29. Knežević, N.Ž.; Durand, J. O.; *Nanoscale*, **2015**, *7*, 2199.
30. Aghabozorg, H.; Daneshvar, S.; Motyeian, E.; Manteghi, F.; Khadivi, R.; Ghadermazi, M.; et al., *J. Iran. Chemi. Soci.*, **2009**, *6*, 620.
31. Eshtiagh-Hosseini, H.; Aghabozorg, H.; Mirzaei, M.; Amini, M.M.; Chen, Y.G.; Shokrollahi, A.; et al., *J. Mol. Struct.*, **2010**, *973*, 180.
32. Soleimannejad, J.; Aghabozorg, H.; Mohammadzadeh, Y.; Nasibipour, M.; Sheshmani, S.; Shokrollahi, A.; et al., *J. Iran. Chem. Soci.*, **2011**, *8*, 247.
33. Shokrollahi, A.; Zamani, R.; *Inorg. Nano-Metal. Chem.*, **2019**, *49*, 127.
34. Ling, Y.; Long, M.; Hu, P.; Chen, Y.; Huang, J.; *J. Hazard. Mater.*, **2014**, *264*, 195.
35. Shao, Y.B.; Jing, T.; Tian, J.Z.; Zheng, Y.J.; Shang, M.H.; *Chem. Pap.*, **2015**, *69*, 1298.
36. Xu, J.; Ju, C.; Sheng, J.; Wang, F.; Zhang, Q.; Sun, G.; et al., *Bull. Korean Chem. Soc.*, **2013**, *34*, 2408.
37. Ulu, A.; Noma, S.A.A.; Koytepe, S.; Ates, B.; *Artificial cells, Nano-Med. Biotech.*, **2018**, *46*, 1035.
38. Khaledyan, E.; Alizadeh, K.; Mansourpanah, Y.; *Iran J. Sci. Technol. Trans. Sci.*, **2019**, *43*, 801.